The Astrophysical Journal, 671:458–469, 2007 December 10

ELECTRONIC AND VIBRATIONAL SPECTROSCOPY OF DIAMONDOIDS AND THE INTERSTELLAR INFRARED BANDS BETWEEN 3.35 AND 3.55 μm

Charles W. Bauschlicher, Jr.,[1] Yufei Liu,[2] Alessandra Ricca,[2]
Andrew L. Mattioda,[2,3] and Louis J. Allamandola[3]
NASA Ames Research Center, Moffett Field, CA 94035
Received 2007 April 12; accepted 2007 August 22

ABSTRACT

The electronic and vibrational spectroscopic properties and ionization energies of diamondoids (nano-diamonds, microdiamonds) are computed using density functional theory (DFT). Spectra of both the neutral and cationic forms of diamondoids, ranging in size from $C_{10}H_{16}$ to $C_{38}H_{42}$, and the IR spectrum of a diamondoid-PAH hybrid molecule are presented. For the 23 neutral species, the C-H stretching bands fall near 3.47 μm and are the strongest in the spectra. Diamondoid ionization energies (IEs) are found to be quite large (about 8 eV). The electronic excitation energies of the neutral species are of the same order as the IEs and have very small oscillator strengths (*f*-values). For the cations, the C-H stretching peak positions differ somewhat from the neutrals and their average integrated band strengths are about half those of the neutrals. The computed electronic excitation energies for the cations are much smaller than those of the neutral species, with *f*-values that are very small. The neutral diamondoids will absorb most strongly near 3.47 μm, which is very close to the position of an absorption band associated with dense clouds that has been tentatively attributed to the tertiary C-H stretch of diamond-like carbon. The spectroscopic properties described here imply that 3 μm emission from highly vibrationally excited diamondoid cations and neutral species should be most intense in regions with strong radiation fields. These results, in conjunction with the observation that the 3.5 μm emission feature originates very close to the exciting star, strongly supports its assignment in HD 97048 and Elias 1 to diamondoid species. While previous work makes an excellent case for large neutral diamondoids, our work shows that some cation contribution cannot be excluded. The very small *f*-values explain why so few sources show this emission.

Subject headings: infrared: ISM — ISM: individual (HD 97048, Elias 1) — ISM: molecules — methods: numerical — ultraviolet: ISM

Online material: color figures

1. INTRODUCTION

Interstellar microdiamonds (Lewis et al. 1987) and polycyclic aromatic hydrocarbons (Basile et al. 1984; Cronin & Chang 1993; Clemett et al. 1993) are found in carbonaceous chondrites. While the interstellar polycyclic aromatic hydrocarbon (PAH) infrared (IR) features dominate the mid-IR emission from most Galactic objects and many extragalactic objects (Cox & Kessler 1999; Peeters et al. 2004; see also ApJS 154, *Spitzer* Supplement) only a very few astronomical objects show spectroscopic features that can be assigned to microdiamonds (Guillois et al. 1999; Van Kerckhoven et al. 2002; Van Kerckhoven 2002; Allamandola et al. 1992, 1993; Pirali et al. 2007). Although the isotopic anomalies of a fraction of the meteoritic diamond prove an extrasolar source, understanding their origin has been challenging. For example, Dai et al. (2002) suggest that nanodiamonds might be formed in the inner solar system. Interstellar PAHs are thought to be formed in the outflows of carbon-rich stars via gas-phase growth mechanisms that are similar to PAH formation in flames. Based on a comparison of meteoritic and terrestrial nanodiamonds Daulton et al. (1996) concluded that meteoritic nanodiamonds are formed by a chemical vapor deposition mechanism, with their growth, perhaps, seeded by C_{60} or C_{70}. However, a gas-phase diamond growth mechanism is not without problems. Consequently, while diamond formation in exotic stellar environments (Jørgenson 1988), interstellar shocks (Tielens et al. 1987), and by quantum heating of small carbonaceous grains (Nuth & Allen 1992) have been suggested, none of these have proven satisfactory (Anders & Zinner 1993; Van Kerckhoven et al. 2002; Van Kerckhoven 2002). Recently, two novel formation mechanisms have been suggested; the first proposes diamondoid growth in ices (Kouchi et al. 2005), while the second proposes their growth in dust gains (Freund & Freund 2006); these mechanisms alleviate some of the difficulties with previous formation mechanisms and warrant serious consideration.

Part of the difficulty associated with tracking interstellar microdiamonds stems from the limited knowledge of their IR spectroscopic and other physical properties. Indeed, although interstellar diamonds were suggested by Saslaw & Gaustad in 1969, it was not until 1993 that the first tentative detection was made. While the spectroscopy of macroscopic synthetic diamonds is well known (Chen et al. 1990; Sandhu et al. 1988; Kobashi et al. 1988), it is not completely applicable to the case of meteoritic and interstellar microdiamonds; the environment of each atom can vary for such small species because the surface to volume atom ratio is close to unity and all bonding electrons are localized. These factors produce an unusual vibrational force field in which each atom vibrates. Furthermore, for microdiamonds, different "crystal" surfaces have similar numbers of atoms, making assignments to a particular structural face difficult. On top of this is the role of hydrogenation and the influence the different faces have on the immediate environment around each

[1] Space Technology Division, Mail Stop 230-3; charles.w.bauschlicher@nasa.gov.
[2] SETI Institute, 515 North Whisman Road, Mountain View, CA 94043.
[3] Astrophysics Branch, MS 245-6.

C-H bond. In addition, Hill et al. (1997, 1998) found that the 21 μm feature depends on the nitrogen content and a 22 μm feature depends on neutron irradiation. The potential spectroscopic modifications brought about by the sometimes harsh chemical separation procedures (Braatz et al. 2000; Mutschke et al. 1995; Jones et al. 2004) further complicates the laboratory study of meteoritic microdiamonds. These issues are well summarized by Van Kerckhoven et al. (2002) and Chang et al. (1995).

Many of the problems associated with the laboratory study of diamondoid molecules were overcome when Dahl et al. (2003) isolated numerous diamondoid species from oil. IR studies of these molecules soon followed (Oomens et al. 2006; Pirali et al. 2007). Using these experimental results along with the associated computational studies, Pirali et al. (2007) were able to make a very convincing assignment of the emission features in the 3.4–3.5 μm region of the spectra of two unique sources, HD 97048 and Elias 1, as arising from neutral diamondoid molecules. They studied molecules up to $C_{87}H_{76}$, and on the basis of the trends they estimated that the interstellar species would have to contain about 130 carbon atoms to provide an adequate fit of the observed intensity ratio of the 3.43 and 3.53 μm bands. They also noted that the non–C-H stretching modes are rather weak in these species. While this is an important step in understanding interstellar diamondoids, they did not consider their electronic spectra, nor did they consider the cations; both are also important in fully understanding the contribution the diamondoids make to the interstellar medium (ISM). To more fully understand the possible contribution diamondoids make to the chemistry and physics of the ISM, we report the IR frequencies and intensities of small diamonds, their cations, and a diamondoid-PAH hybrid molecule. These computationally determined spectroscopic properties, as well as ionization potentials, electronic excitation energies, and oscillator strengths, are presented. Together, these are used to understand the conditions that influence the IR spectroscopic properties of microdiamonds in various interstellar environments and assess their role in diamondoid IR spectroscopy under different interstellar conditions. We should note that these species have been called microdiamonds, nanodiamonds, and diamondoids; in this work we refer to these species as diamondoids, following Dahl et al. (2003), who isolated these species from oil.

The computational methods are presented in § 2, with the results discussed in § 3. The astrophysical applications are presented in § 4.

2. METHODS

The geometries are optimized and the harmonic frequencies and IR intensities are computed using density functional theory (DFT); the B3LYP (Stephens et al. 1994) hybrid (Becke 1993) functional is used in conjunction with the 4-31G basis sets (Frisch et al. 1984 and references therein). The electronic excitation energies and *f*-values are computed using time-dependent DFT (TDDFT; Bauernschmitt & Ahlrichs 1996; Stratmann et al. 1998); we also use the B3LYP functional for these calculations. The calculations are performed using the Gaussian 03 computer codes (Frisch et al. 2003).

In order to compare with the observations, we generate synthetic IR spectra with the full width at half-maximum (FWHM) taken to be 30 cm^{-1}, which is the natural line width of a large molecule emitting under the conditions of the interstellar medium (Allamandola et al. 1989). The intensities are unscaled. In addition to ignoring any variation in line width as a function of mode, Fermi resonances are not accounted for. Despite these limitations, these idealized spectra can be useful in understanding the observed interstellar spectra.

TABLE 1
Diamondoid Names and Formulae

Diamondoid	Name	Formula
D1	Adamantane	$C_{10}H_{16}$
D2	Diamantane	$C_{14}H_{20}$
D3	Triamantane	$C_{18}H_{24}$
D4	[121] Tetramantanes	$C_{22}H_{28}$
D5	P or M [123] Tetramantanes	$C_{22}H_{28}$
D6	[1(2)3] Tetramantanes	$C_{22}H_{28}$
D7	[1212] Pentamantane	$C_{26}H_{32}$
D8	P or M [1213] Pentamantane	$C_{26}H_{32}$
D9	P or M [12(1)3] Pentamantane	$C_{26}H_{32}$
D10	[1(2,3)4] Pentamantane	$C_{26}H_{32}$
D11	[12(3)4] Pentamantane	$C_{26}H_{32}$
D12	P or M [1234] Pentamantane	$C_{26}H_{32}$
D13	3-methyl-[1(2,3)4] Pentamantane	$C_{27}H_{34}$
D14	[12312] Hexamantane (cyclohexamantane)	$C_{26}H_{30}$
D15	[12(1,3)4] Hexamantane	$C_{30}H_{36}$
D16	P or M [12341] Hexamantane	$C_{30}H_{36}$
D17	[12121] Hexamantanes	$C_{30}H_{36}$
D18	P or M [12123] Hexamantane	$C_{30}H_{36}$
D19	[121321] Heptamantane	$C_{30}H_{34}$
D20	[123124] Heptamantane	$C_{30}H_{34}$
D21	[1213](1)21] Octamantane	$C_{34}H_{38}$
D22	[121(2)32(1)3] Nonamantane	$C_{38}H_{42}$
D23	[1231241(2)3] Decamantane	$C_{35}H_{36}$

Notes.—Names and formulae of the 23 diamondoids that are considered here. The numbers in the first column are used in the text and captions to indicate specific diamondoids. The structures are shown in Fig. 1.

This level of theory accurately reproduces the vibrational spectra of neutral and ionized PAHs and is now routinely used to interpret experimental spectroscopic studies (Mattioda et al. 2003) and guide astronomical observations (Hudgins et al. 2005; Malloci et al. 2007). Two recent studies (Oomens et al. 2006; Pirali et al. 2007) focused on the IR spectroscopic properties of neutral diamondoids. In addition to gas-phase spectroscopy of three small diamondoids and the solid state spectra of diamondoid powders, these studies reported DFT calculations for the neutrals. They concluded that the scaled DFT results were in very good agreement with experiment. The optimal scale factor naturally depends on the level of theory and molecules of interest. It is common to have two scale factors, one for the C-H stretch and a second for all other modes. Calibration calculations, which have been carried out for many PAH systems, show that a single scale factor of 0.958 brings the B3LYP harmonic frequencies computed using the 4-31G basis set into excellent agreement with the experimental fundamentals (see, for example, Bauschlicher and Langhoff 1997). In this work, we investigate the optimal scaling factor for diamondoids using adamantane, triamantane, and [12312] hexamantane (cyclohexamantane).

3. RESULTS

The 23 diamondoids listed in Table 1 and shown in Figure 1 are considered in this work. Only the P or M enantiomeric form of the 19 diamondoids described by Dahl et al. (2003) are treated here as these are otherwise equivalent species for the properties considered. The larger species consist of three tetramantanes, seven pentamantanes, five hexamantanes, two heptamantanes, one octamantane, one nonamantane, and one decamantane. The formulae range from $C_{10}H_{16}$ to $C_{38}H_{42}$, and are also given in

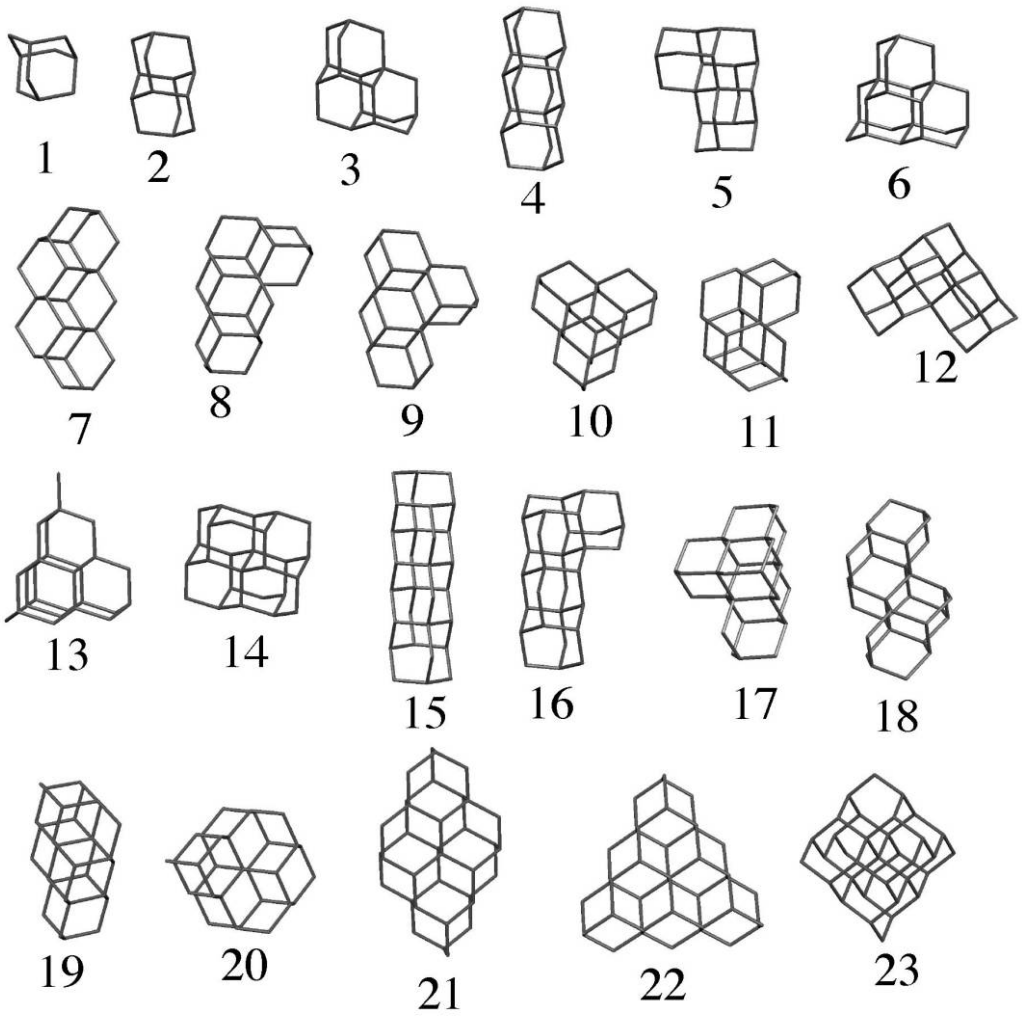

FIG. 1.—The species studied in this work. [*See the electronic edition of the Journal for a color version of this figure.*]

Table 1. For the remainder of this paper, these diamondoids will all be designated by name or table row number. For example, D14 refers to the diamondoid [12312] hexamantane.

3.1. *Calibration*

The level of theory is calibrated using three systems. We use the gas-phase spectrum of adamantane given on the NIST chemistry site Web book,[4] the C-H stretching region of triamantane given by Pirali et al. (2007), and the [12312] hexamantane powder spectrum given by Oomens et al. (2006) as "standards." For adamantane (D1), the strongest band for the unscaled C-H stretching frequency falls at 3036 cm^{-1} (3.293 μm) with an intensity of 509 km $mole^{-1}$ using the 4-31G basis set. This changes to 3041 cm^{-1} (3.288 μm) and 477 km $mole^{-1}$ for the 6-31G* basis and 3053 cm^{-1} (3.275 μm) and 308 km $mole^{-1}$ for the 6-31++G** basis set. These results suggest that our computed 4-31G intensities for the C-H stretch are probably about a factor of 2 too large, as is the case for PAHs (Bauschlicher & Langhoff 1997). Using the same scaling factor (0.958) as in the case of PAHs, the scaled 4-31G frequency of 2908 cm^{-1} (3.439 μm) for the strongest C-H stretching frequency is only 2 cm^{-1} smaller than the NIST experimental gas-phase value. The position of the very weak CH_2 bending mode, determined using the 4-31G basis set, falls at 1484 cm^{-1} (6.738 μm) and differs from experiment by a surprising 54 cm^{-1}. The CH_2 bending mode therefore suggests that the best scale factor for the non–C-H stretches should be 0.923, not 0.958.

A detailed comparison of the experimental spectrum for the C-H stretching region for gas phase triamantane (Pirali et al. 2007) with the computed spectrum, with a FWHM of 10 cm^{-1}, yields a scale factor of 0.9523. Since triamantane is larger than adamantane, it should be more representative of the larger diamondoids and therefore we adopt 0.9523 for the C-H stretching scale factor. Pirali et al. (2007) did not report a detailed spectrum for the CH_2 bending region.

For [12312] hexamantane, using the experimental band positions reported by Oomens et al. (2006) yields 0.943 and 0.953 for the C-H stretching and non–C-H stretching scale factors, respectively. One might be tempted to use the experimentally measured [12312] hexamantane frequencies to determine the scale factors for the diamondoids because it is the largest system experimentally studied, but we note that the Oomens et al. measurements are made on diamondoid powder samples and not on free, individual diamondoid molecules in the gas phase. In the

[4] See http://webbook.nist.gov/chemistry.

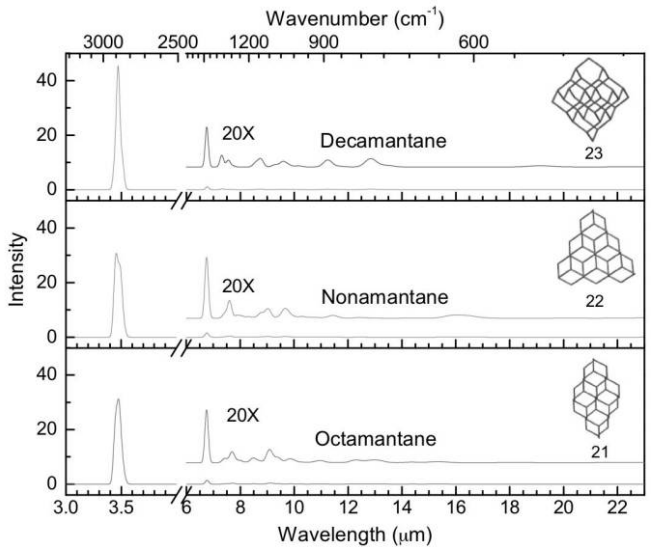

FIG. 2.—The 3–23 μm (3300–435 cm^{-1}) computed spectra of the three largest diamondoids considered here (D21, D22, D23 in Table 1). [*See the electronic edition of the Journal for a color version of this figure*.]

condensed state, adjacent molecules interact, perturbing the vibrational force field and influencing the spectrum. Therefore, we use 0.9523 for the C-H stretching scale factor deduced from the triamantane gas-phase study. However, the spectrum of [12312] hexamantane does not support the CH_2 bending scale factor deduced from adamantane, and we therefore use the value of 0.958 deduced from the PAH data. Finally we should note that for the mixed diamondoid-PAH molecule we use 0.958 for all modes.

3.2. *Neutral Diamondoid Vibrational Spectroscopy*

The IR spectra for all of the neutral diamondoids are very similar, a finding in agreement with Oomens et al. (2006) and Pirali et al. (2007). The mid-IR spectra for the three largest species are shown in Figure 2. The average wavelengths and integrated band intensities (A values) of the strongest bands are summarized in Table 2. As discussed by Pirali et al. (2007), the C-H stretching band is composed of three subbands. Our results are similar, for example, the three bands fall at 3.44, 3.47, and 3.51 μm in decamantane, but at a FWHM of 30 cm^{-1} these three bands merge into one band centered at 3.467 μm. The asymmetric C-H stretch of the CH_2 groups is at the shortest wavelength, the center band is composed of tertiary C-H stretches coupled to the CH_2 symmetric stretch, and the longest wavelength component is due solely to tertiary C-H stretching modes on the face of the diamondoids. Pirali et al. (2007) reported 3.47 μm for the center of the bands in the C-H stretching region. We note that for some species in our sample there is another C-H stretching band (3.396 μm). This seems to be associated with steps in the diamondoid structure where there is an interaction between the C-H stretches on adjacent sites that shift the C-H stretch to even shorter wavelengths. On the basis of the very small average absolute wavelength differences and the maximum differences between C-H stretching band positions listed in Table 2, it is clear that the band positions are nearly constant for all species considered. We should note, however, that Pirali et al. (2007) found that for significantly larger species (up to $C_{87}H_{76}$), the bands shifted to slightly longer wavelengths and the 3.53 μm component increased in intensity relative to the two other components of the 3.47 μm band, thus changing the shape of the band. The average integrated band intensities per C-H for the C-H stretching bands (3.396 and 3.467 μm) shows them to be of similar intensity. The average intensity of the 6.75 μm band is about 5% of the total intensity of the 3.396 and 3.467 μm bands combined.

There are very weak bands in the 20–23 μm range in the neutral species considered here. However, these bands are so weak that with a FWHM of 30 cm^{-1} the bands are not even noticeable in our synthetic spectra as plotted in the figures. The astrophysical band in this region (Hill et al. 1997, 1998) has been attributed to diamondoids. However, as noted by Hill et al. (1998), this band is only present in diamonds with nitrogen impurities, or perhaps after neutron irradiation. Clearly, future extensions of the calculations would be to include some nitrogen or defects in the diamondoids.

3.3. *Neutral Diamondoid Ionization Energies and Electronic Spectroscopy*

The ionization energies (IEs) of several diamondoids are given in Table 3. While the computed IEs have an uncertainty of a few tenths of an eV, the trends should be valid. The IE starts at nearly 9 eV for adamantane and slowly decreases with increasing size of the diamondoid. We suspect that the IE will slowly tend toward the diamond band gap of 5.4 eV. However, from the slow rate of decrease it is clear that the IEs will be large even for very large diamondoids, and we expect large IEs for diamondoids found in the ISM.

The average of the five lowest electronic transitions and corresponding oscillator strengths (f-values) for neutral tetramantane, pentamantane, hexamantane, and decamantane are summarized in Table 4. These diamondoids span the size range of the species considered in this study. While the uncertainty in the excitation energies using TDDFT is commonly assumed to be 0.3 eV, the band positions listed in Table 4 are sufficiently accurate to draw general conclusions about the electronic spectra of these species. First, note that the excitation energies are very large, even for the

TABLE 2

SUMMARY OF IR ACTIVE C-H STRETCHING AND BENDING FUNDAMENTAL VIBRATION WAVELENGTHS AND INTEGRATED ABSORBANCE VALUES

PARAMETER	POSITION (μm)			INTENSITY (km mole^{-1})		
	AVG	AVG-D	MAX-D	AVG	AVG-D	MAX-D
C-H peak in all species	3.467	0.003	0.017	51.3	1.8	5.5
C-H peak in seven species with steps	3.396	0.004	0.008	48.0	6.3	14.1
Weak CH_2 bend in all species	6.753	0.012	0.037	5.5	0.6	1.8

NOTES.—Summary of the IR active C-H stretching and bending fundamental vibration wavelengths (μm) and integrated absorbance values (A, in km mole^{-1}) for the 23 neutral diamondoids considered in this work. These are the strongest bands in the IR spectra of neutral diamondoids. The average (AVG), average absolute deviation (AVG-D) and maximum deviation (MAX-D) are given.

TABLE 3
Summary of Computed Ionization Energies

System	Ionization Energies		
	AVG	AVG-D	MAX-D
Adamantane (D1)	8.94	...	...
Diamantane (D2)	8.41	...	...
Triamantane (D3)	8.08	...	...
Tetramantane (D4–D6)	7.86	0.03	0.04
Pentamantane (D7–D13)	7.68	0.06	0.12
Hexamantane (D14–D18)	7.51	0.05	0.12
Decamantane (D23)	7.34	...	...

Notes.—Summary of computed ionization energies (IE), in eV, for seven diamondoids spanning the size range of the species in Table 1. The average IE (AVG), average absolute deviation (AVG-D), and maximum deviation (MAX-D) are given.

largest species. Hovering around 8 eV, they are slightly larger than the ionization energies (Table 3). In addition, the *f*-values are very small, much smaller than those for neutral PAHs (Halasinski et al. 2003).

3.4. *Diamondoid Cation Vibrational Spectroscopy*

For the diamondoid species, all the valence electrons occupy bonding orbitals and remain localized in the individual C-C bonds.

TABLE 4
Average Electronic Band Positions and Oscillator Strengths

State	ΔE			f		
	AVG	AVG-D	MAX-D	AVG	AVG-D	MAX-D
Tetramantane (D4–D6)						
1	7.73	0.01	0.01	0.003	0.003	0.005
2	7.82	0.13	0.20	0.003	0.003	0.005
3	8.06	0.06	0.09	0.006	0.008	0.012
4	8.36	0.11	0.17	0.011	0.008	0.011
5	8.42	0.07	0.10	0.009	0.004	0.007
Pentamantane (D7–D13)						
1	7.61	0.04	0.07	0.003	0.002	0.003
2	7.69	0.08	0.21	0.003	0.002	0.004
3	7.83	0.17	0.22	0.006	0.004	0.006
4	8.21	0.14	0.27	0.003	0.003	0.006
5	8.26	0.11	0.21	0.010	0.008	0.022
Hexamantane (D14–D18)						
1	7.49	0.06	0.12	0.000	0.001	0.001
2	7.60	0.10	0.14	0.003	0.003	0.009
3	7.80	0.11	0.18	0.002	0.002	0.003
4	8.01	0.06	0.14	0.010	0.011	0.021
5	8.08	0.07	0.10	0.007	0.005	0.008
Decamantane (D23)						
1	7.21	...	...	0.000	...	...
2	7.86	...	...	0.000	...	...
3	7.88	...	...	0.000	...	...
4	8.15	...	...	0.260	...	...
5	8.16	...	...	0.000	...	...

Notes.—The average electronic band positions (in eV) and oscillator strengths (*f*-values) of the five lowest excitations for four neutral diamondoids. The average band position (AVG), average absolute deviation (AVG-D), and maximum deviation (MAX-D) are given.

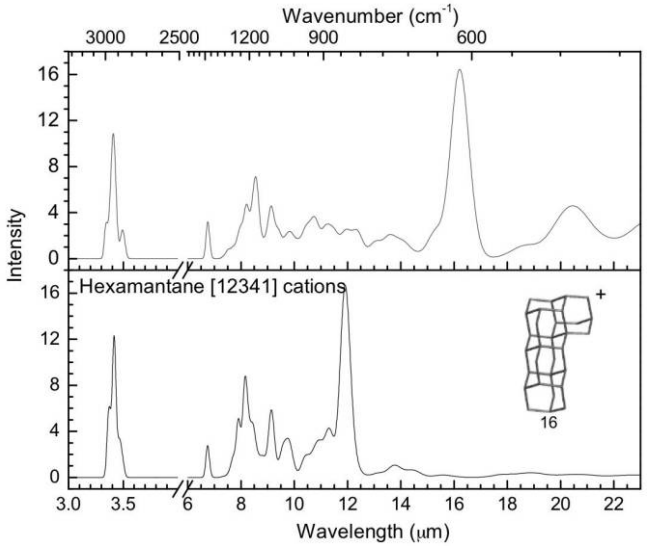

Fig. 3.—The 3–23 μm (3300–435 cm^{-1}) computed spectra of two states of the [12341] hexamantane cation (D16 in Table 1). [*See the electronic edition of the Journal for a color version of this figure.*]

Therefore on ionization one or a few of the C-C bonds weakens, and as expected the length of those particular bonds increases. This is in sharp contrast with the behavior of PAH ions, where the highest lying bonding electrons are delocalized and the charge is spread over the entire carbon network. Consequently, ionization of a PAH molecule effects the vibrational force field of the whole molecule, not just one or a few individual C-C bonds as found for the diamondoids. Because there are many nonequivalent C-C bonds in diamondoids, there are several distinct low-lying states of the cations for the same diamondoid. We do not fully explore all of the possible diamondoid cation states for each species, but rather optimize the geometry of the cation starting from the neutral geometry and orbitals. However, for some species we optimized the cations starting from different geometries and found several different cation states that are close in energy. Different C-C bonds can be ionized in a particular diamondoid cation, with the charge remaining localized on that bond. Consequently, the different cation states for that diamondoid cation show some important differences in the fundamental C-C stretching vibrations. In Figure 3 we show the spectra of two states of the [12341] hexamantane cation that differ in energy by about 3 kcal mole^{-1} (0.12 eV); these two spectra show larger differences than found for different states of other diamondoids. While the C-H stretch and CH_2 bending band positions are very similar (the maximum difference of the C-H stretching bands in these 2 cation states is 6 cm^{-1}), there are very large changes in the 10–18 μm region. Because these diamondoid cation structures are similar in energy, the IR spectra for a mixture of these species will likely be an average of the spectra of the low-lying cation states. It is also possible that the cations could lose a hydrogen atom to improve the C-C bonding. The loss of an H atom for a PAH cation was found (Jolibois et al. 2005) to be favored over the loss of H_2, and we suspect this will also be true for the diamondoids.

Because of these uncertainties, what is reported here for diamondoid spectroscopy at longer wavelengths should be considered as preliminary, and if diamondoid cations are tentatively identified in the ISM, more calculations and experiments are called for. Due to the differences at longer wavelengths, we focus on the wavelengths of the C-H stretching and CH_2 bending

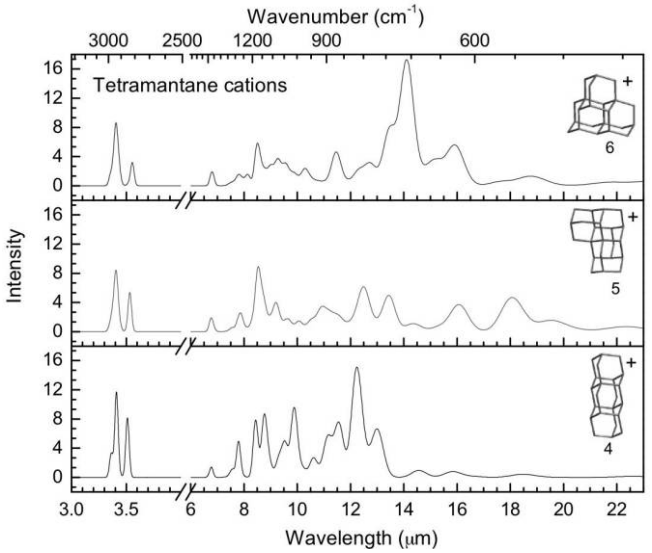

FIG. 4.—The 3–23 μm (3300–435 cm^{-1}) computed spectra of the three tetramantane cations, D4–D6 in Table 1. [*See the electronic edition of the Journal for a color version of this figure.*]

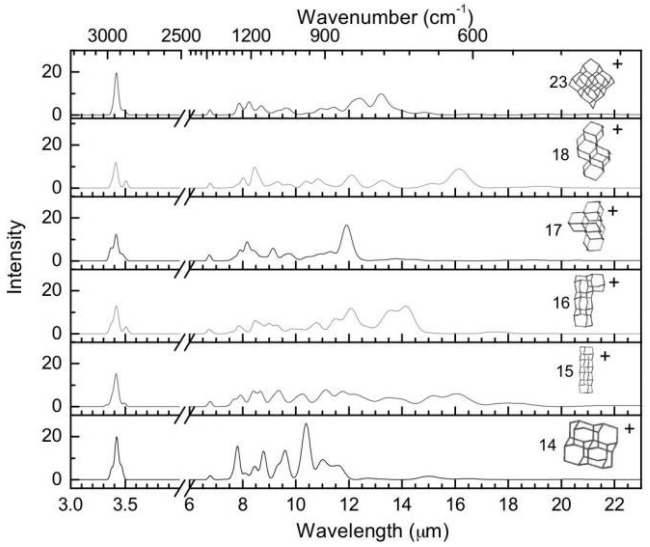

FIG. 6.—The 3–23 μm (3300–435 cm^{-1}) computed spectra of the decamantane cation (D23) and the five hexamantane cations, D14–D18, listed in Table 1. [*See the electronic edition of the Journal for a color version of this figure.*]

vibrations since they remain consistent for the different cation states found.

In Figures 4, 5, and 6 we show the computed mid-IR spectra of the tetramantane, pentamantane, hexamantane, and decamantane cation species considered in this work. The C-H stretching peak positions and the average integrated band strength per C-H for the C-H stretching bands (3.376, 3.432, and 3.527 μm) are summarized in Table 5. Comparison with Table 2 shows that, on ionization, there is a small shift in the position of the strongest band and that an additional prominent feature appears at 3.527 μm. As for the neutrals, the spectra in the C-H stretching region are rather constant regardless of diamondoid structure and size. Individual C-H stretch band intensities decrease by about a factor of 2 on ionization. For example, the total integrated intensity in the C-H stretching region of neutral decamantane is 298 km mole^{-1}, compared with 152 km mole^{-1} for the cation. Excluding the weak feature near 6.75 μm produced by the CH_2 bending vibration, the remaining spectral features show significant variations between different diamondoid species and within diamondoid families. That is, while the band positions fall in the regions expected for single-bonded C-C stretching and bending vibrations and C-H wags, they vary from diamondoid to diamondoid. Furthermore, the intensity of a given band can also vary between the different species considered. Thus the spectra of a larger number of diamondoid cations would be rather featureless at wavelengths longer than 6.75 μm. As discussed in § 4, the absence of characteristic diamondoid vibrational frequencies in the 5–16 μm region that do not vary much from molecule to molecule would appear to make it much more difficult to detect and characterize diamondoid cations in the interstellar medium than it has been for PAHs.

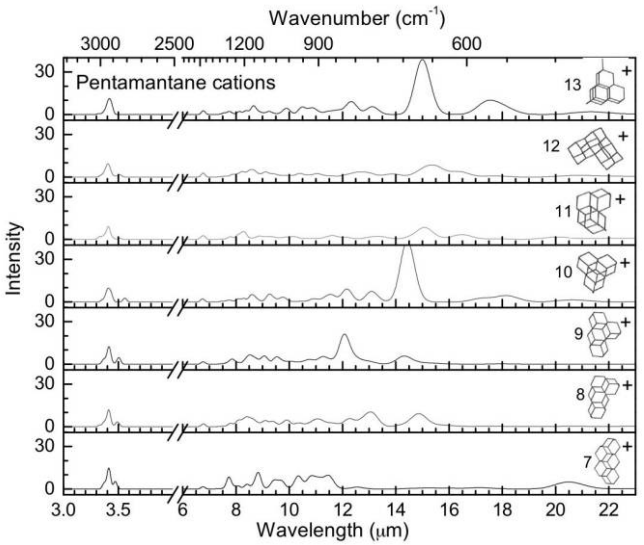

FIG. 5.—The 3–23 μm (3300–435 cm^{-1}) computed spectra of the seven pentamantane cations, D7–D13, listed in Table 1. [*See the electronic edition of the Journal for a color version of this figure.*]

3.5. *Diamondoid Cation Electronic Spectroscopy*

The 10 lowest electronic transition energies and *f*-values computed for the tetra-, penta-, hexa-, and decamantane cations are listed in Table 6. Since these are radical cations with a low-lying partly filled orbital, there is a significant reduction in the excitation energies with respect to their neutral counterparts (Table 4). Consequently, these diamondoid cation transitions fall roughly between 1 and 2 eV, whereas the transition energies for the lowest lying transitions in their neutral counterparts are in the vicinity of 8 eV. As with the neutrals, the *f*-values for these transitions are very small and these species are also not expected to be strong absorbers of optical radiation. Given that both the neutrals and cations are weak absorbers in the UV-visible-NIR spectral range, we can expect that, even if interstellar diamondoids are as abundant as interstellar PAHs, they will emit weakly at best and will therefore be much more difficult to observe in emission (e.g., see Mattioda et al. 2005). In fact, as discussed in § 4, it is far more likely that they contribute to interstellar absorption spectra rather than emission spectra.

3.6. *The Infrared Properties of the Diamondoid-PAH Hybrid: Pyrene-triamantane*

We also computed the spectrum of a covalently bonded diamondoid-PAH system. Jones & d'Hendecourt (2000) suggested

TABLE 5
SUMMARY OF STRONGEST IR ACTIVE C-H STRETCHING AND BENDING FUNDAMENTAL VIBRATION WAVELENGTHS AND INTEGRATED ABSORBANCE VALUES

	Position (μm)			Intensity (km mole^{-1})		
Parameter	AVG	AVG-D	MAX-D	AVG	AVG-D	MAX-D
Main peak in all species	3.432	0.003	0.011	21.3	2.2	5.6
Lower frequency band	3.376	0.006	0.020	17.4	3.3	111.3
Higher frequency band	3.527	0.019	0.053	45.3	23.2	84.7
CH_2 bend	6.770	0.009	0.029	9.1	1.7	3.6

NOTES.—Summary of the strongest IR active C-H stretching and bending fundamental vibration wavelengths (μm) and integrated absorbance values (A, in km mole^{-1}) for the 20 diamondoid cations D4–D18 and D23. The average (AVG), average absolute deviation (AVG-D), and maximum deviation (MAX-D) are given.

that interstellar radiation could lead to a reconstruction of the diamondoid surfaces, leading to an sp^2 hydrogenated configuration. These surface reconstructed nanodiamonds are particles with both diamondoid (sp^3) and aromatic (delocalized sp^2) character. As suggested by Jones & d'Hendecourt (2000), since pure diamondoids are not strong absorbers of optical radiation, such mixed species could be important in exciting diamondoid emission, with the aromatic portion of the molecule acting as an antenna for the pumping excitation. Once the aromatic moiety becomes highly excited, the vibrational energy is quickly shared with the diamondoid portion of the structure and, provided it is small enough, the particle will emit at all the allowed fundamental vibrational frequencies of the PAH and diamondoid structures of which it is comprised.

Consider the spectroscopic properties of the merged pyrene-triamantane system. The specific molecule treated here is shown in Figure 7. Clearly this is only one of many possible hybrid species, where the PAH coverage can go from one molecule all the way to a diamondoid that is completely covered with PAHs. In Figure 8 the computed IR spectra of triamantane, pyrene, and the merged system are presented. With the exception of the bands at 12 and 13.1 μm, the spectrum of the merged system looks like the superposition of the triamantane and pyrene spectra. The 12 μm band for the merged system corresponds to the C-H out-of-plane (CHoop) bending vibrations of the duo hydrogens on the pyrene moiety. Replacing two of the duo H atoms in pyrene with the C-C bridging bonds to triamantane shifts the duo hydrogen vibration from 11.8 to 12 μm. Likewise, this also shifts the 13.4 μm pyrene CHoop band to 13.1 μm. The spectrum of the merged system in the C-H stretching region (see Fig. 8) also appears as the superposition of the separate systems. Thus while the C-H stretching region can differentiate between PAHs and diamondoids, if diamondoid-PAH hybrid species with low PAH coverage exist, it would probably be difficult to separate their features from a mixture of PAHs and diamondoids because the shift in the out-of-plane bending modes is consistent with the variation in position between different PAHs. As discussed in § 4.3, the only IR spectroscopic tracer of such low PAH coverage, mixed species, would be much stronger diamondoid IR emission than can be explained by their small UV cross sections.

4. ASTROPHYSICAL APPLICATIONS

Here we discuss some astrophysical implications of the results presented above. We note that our discussion is limited to pure diamondoid species, as there is experimental evidence that nitrogen impurities or neutron irradiation of diamonds will introduce a 21 μm band (Hill et al. 1998) and could also result in other changes in the properties discussed in this work. The possibility of detecting the IR signature of neutral and ionized diamondoids in different astronomical settings is considered. The situation appears similar to that which holds for interstellar PAHs, but is far more constrained. Some interstellar conditions strongly favor absorption, whereas others clearly favor emission. Lastly, the question of diamondoid formation is revisited.

4.1. *The IR Signature of Neutral Interstellar Diamondoids*

The mid-IR spectra of neutral diamondoids in Figure 2 show that the C-H stretching bands provide the best chance of detection in most astronomical environments. With A values of about 50 km mole^{-1} (Table 2), the 3.40 and 3.47 μm diamondoid bands are the strongest in the mid-IR. In addition, the lowest energy electronic transitions in these neutral species fall near 8 eV, slightly above their ionization energies, and their oscillator strengths are very small. With some exceptions, most f-values are only a few thousandths. Thus, in most astronomical environments, if diamondoids are present, the majority would be in the neutral form. Furthermore, if neutral diamondoids are indeed abundant in the ISM, these spectroscopic properties favor detection by absorption rather than emission. The combination of small f-values and 8 eV excitation energies makes it unlikely that, as a class, neutral diamondoids can become sufficiently excited to emit strongly in the IR. Compare this with the properties of the PAHs responsible for the well-known interstellar mid-IR emission features. With f-values that approach unity, absorptions which span the UV through the NIR (e.g., Mattioda et al. 2005), and IR transitions with A values of several hundred km mole^{-1} (e.g., Bauschlicher 2002), PAHs are orders of magnitude more efficient at every step in the IR excitation/emission process than are neutral diamondoids. Nonetheless, it is possible that interstellar diamondoids could produce some weak emission near 3.47 μm. Indeed, many very weak bands have been detected in this region superposed on a broad emission plateau spanning the 3.25–3.5 μm range (Jourdain de Muizon et al. 1990; Allamandola et al. 1989) A number of plausible candidates for these weak features have been suggested over the years and, as discussed by Van Kerckhoven et al. (2002), diamondoids could certainly be among these.

The calculations presented here predict that, across the entire IR spectral range, neutral diamondoids will absorb most strongly near 3.47 μm. This is very close to the position of an absorption band associated with dense clouds that has been tentatively attributed to the tertiary C-H stretch of diamond-like carbon (Allamandola et al. 1992, 1993; Brooke et al. 1996, 1999). This broad absorption feature is superposed on, and severely blended with, the long wavelength wing of the 3 μm H_2O ice band. This feature peaks at about 3.47 μm and has a full width at half height (FWHH) that, depending on the object, varies between 0.05 and 0.1 μm. The broad interstellar feature encompasses the major

TABLE 6
AVERAGE ELECTRONIC BAND POSITIONS AND *f*-VALUES

	ΔE			*f*		
STATE	AVG	AVG-D	MAX-D	AVG	AVG-D	MAX-D
Tetramantane (D4–D6)						
1	0.79	0.07	0.11	0.001	0.001	0.001
2	1.10	0.06	0.08	0.000	0.000	0.000
3	1.41	0.01	0.01	0.020	0.013	0.019
4	1.51	0.02	0.03	0.019	0.004	0.006
5	1.63	0.03	0.05	0.016	0.010	0.014
6	1.77	0.07	0.11	0.019	0.022	0.033
7	1.91	0.03	0.05	0.001	0.001	0.001
8	2.25	0.09	0.14	0.002	0.002	0.003
9	2.41	0.13	0.19	0.054	0.070	0.105
10	2.58	0.05	0.08	0.002	0.002	0.003
Pentamantane (D7–D13)						
1	0.78	0.10	0.19	0.001	0.001	0.001
2	0.95	0.20	0.35	0.001	0.001	0.002
3	1.34	0.07	0.12	0.019	0.010	0.013
4	1.43	0.12	0.20	0.022	0.008	0.022
5	1.58	0.05	0.09	0.013	0.010	0.020
6	1.70	0.06	0.12	0.019	0.024	0.085
7	1.82	0.13	0.24	0.002	0.002	0.007
8	2.19	0.13	0.30	0.003	0.003	0.011
9	2.28	0.07	0.17	0.032	0.036	0.085
10	2.39	0.08	0.17	0.025	0.024	0.065
Hexamantane (D14–D18)						
1	0.82	0.08	0.11	0.001	0.001	0.002
2	1.06	0.14	0.27	0.002	0.002	0.004
3	1.31	0.05	0.08	0.022	0.015	0.023
4	1.42	0.07	0.17	0.024	0.020	0.051
5	1.55	0.06	0.10	0.015	0.007	0.015
6	1.66	0.05	0.10	0.053	0.070	0.174
7	1.77	0.07	0.10	0.005	0.006	0.015
8	2.06	0.15	0.25	0.002	0.002	0.005
9	2.18	0.11	0.21	0.016	0.020	0.051
10	2.29	0.13	0.18	0.015	0.017	0.039
Decamantane (D23)						
1	0.76	...	...	0.000	...	...
2	0.76	...	...	0.000	...	...
3	1.22	...	...	0.027	...	...
4	1.23	...	...	0.027	...	...
5	1.36	...	...	0.000	...	...
6	1.40	...	...	0.001	...	...
7	1.40	...	...	0.001	...	...
8	2.06	...	...	0.001	...	...
9	2.27	...	...	0.000	...	...
10	2.27	...	...	0.000	...	...

NOTES.—The average electronic band positions (in eV) and *f*-values of the 10 lowest excitations for five diamondoid cations. The average (AVG), average absolute deviation (AVG-D), and maximum deviation (MAX-D) for the band positions are given.

3.47 μm band predicted here, as well as that reported by Oomens et al. (2006) for powdered diamondoid samples (3.47 μm), Pirali et al. (2007) for gas-phase diamondoids, and Chin et al. (1992) for the C-H stretch on the diamond C(111) surface. Severe blending with the absorption bands from other interstellar ice constituents obscures the region near 3.4 μm, the position of another diamondoid C-H stretch band. The suggestion that this interstellar feature originates in diamonds has been questioned because it appears to scale with the H_2O ice band, behavior expected of volatile material trapped within the ice rather than a refractory substance such as bulk diamond (Brooke et al. 1996, 1999). However diamondoids, like PAHs, are large molecules and could be frozen into ice grain mantles as are the PAHs. Thus their absorptions would track with the H_2O ice band as do the other species frozen in the ice mantles. Another rationalization in favor of a diamondoid origin of this feature is the abundance implied. In our earlier work we assumed an *A* value of 24 km mole^{-1} per C-H, appropriate for tertiary carbon, and deduced that between 2% and 6% of cosmic carbon was in the form of the tertiary C-H tentatively attributed to interstellar "diamonds." Above we show that the average *A* value for tertiary C-H in the diamondoids is 51 km mole^{-1}, a value that is double that used earlier. Doubling the integrated absorbance value is equivalent to halving the fraction of cosmic carbon present in the tertiary form. This implies that only about 1%–3% of the cosmic C is necessary to account for this band, since the surface to volume carbon atom number for these diamondoids is generally greater than one. Furthermore, since neutral diamondoids have very weak absorption

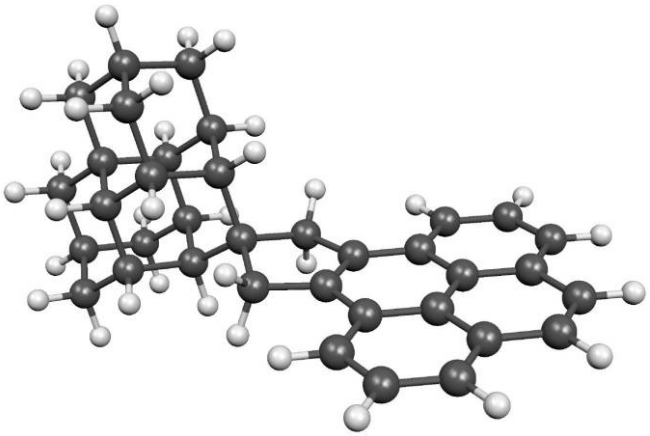

FIG. 7.—Mixed pyrene-triamantane system. [*See the electronic edition of the Journal for a color version of this figure*.]

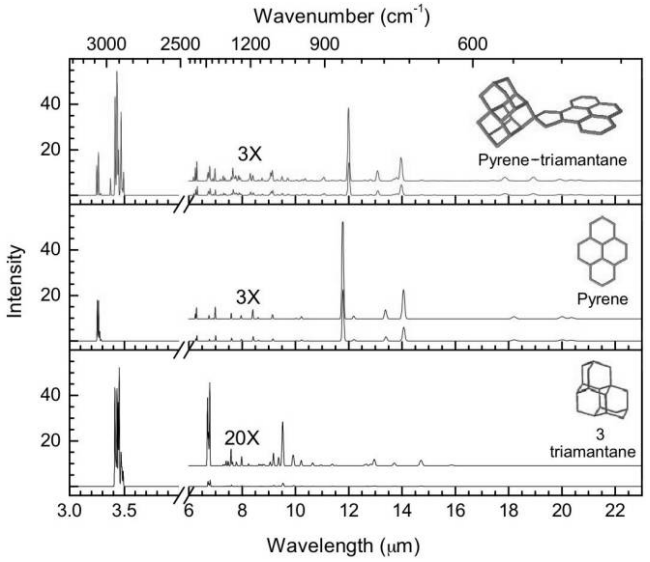

FIG. 8.—The 3–23 μm (3300–435 cm^{-1}) computed spectra of pyrene, triamantane, and the pyrene-triamantane hybrid species shown in Fig. 7. [*See the electronic edition of the Journal for a color version of this figure*.]

outside of the C-H stretching region, 1%–3% of the carbon in this form would not impact other regions of the spectrum. Thus, the data presented here and the data presented by Oomens et al. (2006) and Pirali et al. (2007) continue to favor a diamondoid origin of the interstellar 3.47 μm band.

4.2. *The IR Signature of Interstellar Diamondoid Cations*

The mid-IR spectra of diamondoid cations differ significantly from that of their neutral counterparts. Figures 4–6 show that, although the bands in the 6–16 μm range are strong, they vary in both peak position and relative band strengths and, as discussed in § 3.4, if one includes the contribution from excited states there are even larger variations. This absence of characteristic diamondoid cation vibrational frequencies in the 5–16 μm region precludes their use as a reliable probe for interstellar diamondoids. It is possible that, on losing or gaining hydrogen atoms, the spectral variation would be reduced, but this introduces a dramatic increase in the number of species that need to be considered. Proper treatment of that is beyond the scope of this paper and we defer that question to the future.

On the other hand, the bands in the 3 μm region are quite reproducible and can be used as a diamondoid cation tracer in astronomical absorption and emission spectra. Regarding absorption, comparing the band strengths for the neutral species listed in Table 2 with those for the cations in Table 5 shows that the *A* values for the diamondoid cation C-H stretching bands are somewhat smaller than those of the corresponding neutrals. Comparing the peak positions of these bands with the broad interstellar absorption band discussed above shows they too could contribute to this feature. Indeed, the presence of cations within interstellar ices has been invoked to provide the charge balance required by OCN^- (Schutte & Greenberg 1997; Demyk et al. 1998). Furthermore, the ionization potential for PAHs trapped in water ice is reduced by 2 eV (Gudipati & Allamandola 2004) by a mechanism that should be applicable for trapped organics in general (Woon & Park 2004). As with the 3.4 μm component, other ice constituents such as CH_3OH and H_2CO absorb near 3.5 μm and could easily screen the strong diamondoid cation feature near 3.5 μm.

For emission, the spectroscopic properties of diamondoid cations place tight constraints on the possible locations in which they can be detected via the IR fluorescence process. While their electronic transition energies (Table 6) are much lower than those of the neutral species (Table 4), enabling them to harvest radiant energy from the UV through the NIR, the corresponding oscillator strengths are quite low. Thus, if diamondoid cations are present in sufficient abundance in the ISM, the low *f*-values spanning the UV through the NIR limit the excitation rate. Furthermore, the richness of the IR spectrum longward of 6 μm increases the efficiency of the relaxation process. Taken together, these spectroscopic properties suggest that 3 μm emission from highly vibrationally excited diamondoid cations should be most intense in regions with strong radiation fields. The strength of the predicted diamondoid cation bands longward of 6 μm suggests an observational test of their contribution to the emission spectra of HD 97048 and Elias 1. If present in sufficient quantity, the cations would produce unusual features in the 5–10 μm region of the spectrum that would drop with distance from the exciting stars.

4.3. *The IR Signatures of Interstellar Diamondoid-PAH Merged Species*

Here the possibility of detecting IR signatures that arise from molecule-sized hybrid species containing both diamondoid and aromatic subgroups is considered. The case for emission is treated first. As discussed in § 3.6, the ability of the aromatic moiety to efficiently absorb optical radiation spanning the UV through NIR (Mattioda et al. 2005) would produce highly vibrationally excited hybrid particles in a manner similar to that which holds for interstellar PAHs. As shown in Figure 8, vibrational relaxation of these species with low PAH coverage will produce emission spectra with bands characteristic of both diamondoids and aromatic species. Consequently, if such species were as widespread and as abundant as the PAHs, one would expect to see some correlation and comparable intensities between the 3.3 μm PAH C-H stretch band and the diamondoid C-H stretching features listed in Tables 2 and 5. This generally is not the case. However, observations cannot rule out the presence of such interstellar species. Although emission from PAHs and PAH-related species can accommodate the 3.3 μm band and perhaps much of the underlying plateau, relaxation from vibrationally excited C-H stretches in diamondoid-PAH hybrids could contribute to the emission plateau and the well-known bands superposed on this plateau at these frequencies. Thus it is not currently possible to distinguish between separate or merged interstellar species on the basis of either emission or absorption.

4.4. *Diamondoids and Interstellar IR Spectroscopy from* 3.35 *to* 3.6 μm

Summing up, the data presented here indicates that interstellar diamondoids can only be traced in the 3 μm region. Neutral diamondoids contribute very little at longer wavelengths. For emission, electronic spectral properties argue against the efficient optical excitation-IR fluorescence mechanism that holds for PAHs. Rather, diamondoid optical properties require high-energy photons and high flux to attain sustained and significant vibrational excitation. On the other hand, both neutral and charged diamondoids can contribute to the weak absorption band near 3.47 μm that can be detected in lines of sight that sample dense clouds. A similar situation holds for PAHs. A very weak absorption band at 3.3 μm that is superposed on the long wavelength side of the strong H_2O ice absorption feature has been attributed to PAHs (Brooke et al. 1996, 1999; Sellgren et al. 1995; Bregman & Temi 2001).

Figure 9 compares the interstellar IR emission from 3.35 to 3.6 μm that has been attributed to diamonds (Guillois et al. 1999; Van Kerckhoven et al. 2002; Van Kerckhoven 2002) with a schematic of the absorption feature associated with diamonds in dense clouds, and the computed neutral and cation diamondoid C-H stretch bands presented here. Seen clearly in only two objects to date, HD 97048 and Elias 1, the emission spectra in Figures 9*a* and 9*b* are very rare. Furthermore, the unusual 3.5 μm emission band originates very close to the exciting source. Roche et al. (1986), using speckle interferometry, showed that the strong 3.53 μm feature emission zone in HD 97048 is less than 0.05″ from the star, in sharp contrast with the PAH emission features which are extended over vast distances around this object. In a very recent, high angular resolution study, Habart et al. (2006) suggest that the diamond emission is confined to the disk surrounding HD 97048. Similarly, as discussed in Van Kerckhoven et al. (2002) and Van Kerckhoven (2002), the 3.53 μm emission zone associated with Elias 1 is constrained to less than 0.15″ from the exciting star. See Topalovic et al. (2006) for a comparison of the spatial distribution of both the diamondoid and PAH emission features associated with Elias 1. In both cases, the central stars are thought to be HAeBe stars (Van Kerckhoven et al. 2002; Van Kerckhoven 2002). We should note that Pirali et al. (2007) found that for neutral diamondoids larger than those considered

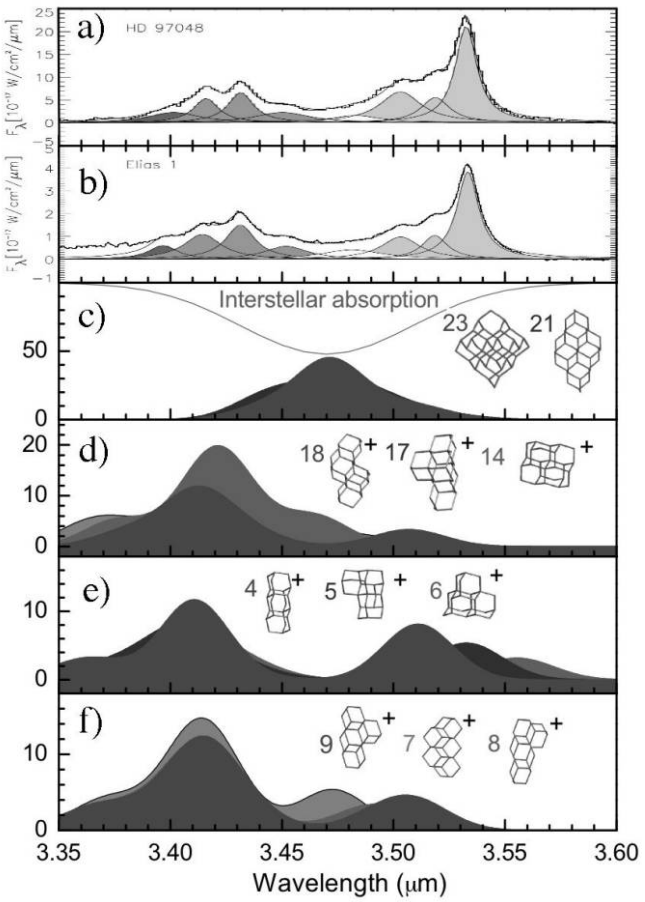

FIG. 9.—The 3.35–3.60 μm region of the spectrum from HD 97048 and Elias 1 compared with a schematic of the interstellar absorption feature associated with dense molecular clouds and the spectra of neutral and ionized diamondoids computed here. The computed spectra have a FWHM of 30 cm^{-1}. The spectra of HD 97048 and Elias 1 are reproduced from Van Kerckhoven et al. (2002) and Van Kerckhoven (2002). Note that the neutral diamondoid spectra shown in (*c*) do not contain step surfaces and therefore the 3.4 μm feature is not present. [*See the electronic edition of the Journal for a color version of this figure.*]

in our work, the 3.53 μm band increased in intensity with respect to the other components of the 3.47 μm band, giving neutral diamondoids a band shape more similar to those of HD 97048 and Elias 1. However, as shown in Figure 9, it is impossible to rule out some cation contribution as well, which would be consistent with the strong radiation field very close to the stars. Contributions from diamondoid cations to the emission can be probed by measuring the 5–20 μm spectra close to the exciting stars in HD 97048 and Elias 1. Since diamondoid cations have very strong bands in this region, if they are indeed present, they should add unusual features to the emission spectra close to the star, features that diminish with respect to the PAH bands with distance from the star.

The close proximity of the diamondoid emission bands to the exciting star, in contrast with the widespread PAH emission features, is in keeping with the diamondoid photophysics discussed above. The low *f*-values, combined with the narrow UV absorption intrinsic to diamondoids, limits IR fluorescence to dusty regions which experience both high-energy and high-flux UV radiation fields. These tight constraints on the diamondoid emission process, coupled with the evidence that the far more common, but weak, 3.47 μm absorption band associated with dense clouds is due to diamondoids, suggest that interstellar diamondoids could be as widespread as interstellar PAHs.

4.5. *The Growth of Diamondoids*

As noted in the introduction, recently two new diamondoid growth mechanisms have been proposed that seem to alleviate some of the problems with previous gas-phase models. Kouchi et al. (2005) suggested that diamondoids are formed in irradiated ices. In their experiments they formed diamond and graphite adjacent to each other. Their mechanism would therefore seem to support both the formation of pure diamondoid as well as mixed diamondoid-PAH species, of the type suggested by Jones and d'Hendecourt (2000). If formed in ices, this would also explain the correlation between the 3.47 μm and the water band.

Freund & Freund (2006) proposed the formation of organics under pressure inside a silicate grain. They noted that the intensity ratio of the 9.7 μm silicate feature to the 3.4 μm band in the diffuse ISM is approximately 10 : 1 and suggested that this supported the formation of some classes of organic materials in the silicate grains. They noted that in dense clouds the 3.4 μm band characteristic of the diffuse ISM is replaced by the 3.47 μm band. Our assignment for the 3.47 μm band to neutral diamondoids suggests that diamondoids might be one of the species forming in the silicate grains. However, the observation that 3.4 μm band is not polarized (Adamson et al. [1999] and more recently Chiar et al. [2006]), while the 10 μm silicate band and 3 μm ice feature are, suggests that the diamondoids are observed in the gas phase. That is, if they are formed in the ices or silicates, they are being observed in gas phase. If the growth of diamondoids occurs in crystals, similar mixed diamondoid-PAH species can also be formed, especially if the carbon species were freed from the crystal before the growth process was completed. Finally, we should note that if the mixed diamondoid-PAHs are not formed with the diamondoids, it is also possible that reactions between PAHs and diamondoids could form such species, especially in energetic regions where the loss of H atoms could promote the bonding between such species. It would be interesting to see a theoretical study of the reaction barriers for the fusion of diamondoids and PAHs.

While the growth of interstellar diamondoids in ices or in silicates is speculative, these new formation methods should be seriously considered, as they appear to alleviate some of the problems associated with the previously proposed gas-phase mechanisms.

5. CONCLUSIONS

The electronic and vibrational spectroscopic properties and ionization energies of diamondoids have been computed using density functional theory (DFT). Infrared spectra of both the neutral and cationic forms of diamondoids, ranging in size from $C_{10}H_{16}$ to $C_{38}H_{42}$, and the IR spectrum of a diamondoid-PAH hybrid molecule are presented.

The computed vibrational spectra of the neutral diamondoids are in good agreement with experiment. The spectra of the 23 neutral diamondoids show that the strongest bands originate from the C-H stretch, with the peak position falling at 3.47 μm. The CH_2 bending vibration at 6.75 μm is much weaker. Band positions are essentially constant for all neutral species considered. Ionization of these species requires more than 7 eV. The electronic excitation energies of the neutral species are of the same order as the IEs and are typically very weak, with *f*-values in the thousandths.

The IR spectra of 15 diamondoid cations of different sizes and structures were also computed. While the positions for the diamondoid cation C-H stretching bands are nearly constant,

they are somewhat different from those of the neutrals and fall at 3.376, 3.432, and 3.527 μm. On ionization, the strength of the C-H stretching band is typically halved. Excluding the weak feature near 6.75 μm produced by the CH_2 bending vibration, the remaining long wavelength spectral features show significant variations between different diamondoid cations and within diamondoid families. Some of these bands can be stronger than those between 3.35 and 3.55 μm. The electronic excitation energies for diamondoid cations are much smaller than those of the neutral species, with very small *f*-values.

These spectroscopic properties imply that if diamondoids are present in most astronomical environments, the majority would be in the neutral form. The combination of small *f*-values and 8 eV excitation energies makes it unlikely that, as a class, neutral diamondoids can become sufficiently excited to emit strongly in the infrared in most astronomical environments. Thus, if neutral diamondoids are abundant in the ISM, their spectroscopic properties favor detection by absorption in the 3 μm region rather than emission. The calculations presented here predict that, across the entire IR spectral range, neutral diamondoids will absorb most strongly near 3.47 μm. This is very close to the position of an absorption band associated with dense clouds that has been tentatively attributed to the tertiary C-H stretch of diamond-like carbon. Thus, the data presented here and the data presented by Oomens et al. (2006) and Pirali et al. (2007) continue to favor a diamondoid origin of the interstellar 3.47 μm absorption band. Given their high electronic transition energies and small *f*-values, interstellar diamondoids could contribute weak structure to the broad plateau underlying the strong 3.3 μm PAH emission feature.

The electronic spectroscopic properties of both neutral and ionized diamondoids place tight constraints on the astronomical environments in which they can become sufficiently excited to emit strongly in the IR. If diamondoids are widespread throughout the ISM, the very small *f*-values of their electronic transitions explain why so few sources show this emission. Clear-cut IR fluorescent emission from highly vibrationally excited diamondoid cations and neutral species requires radiation fields with both high energy and high flux. The results presented here are consistent with the observation that the rare 3.5 μm interstellar emission feature originates very close to the exciting star.

As demonstrated by Pirali et al. (2007), as the neutral diamondoids grow larger in size, there is an increase in the 3.53 μm component of the 3.47 μm band. The increase in the 3.53 μm component is consistent with the observation of a similar band in bulk diamond. This increase in the 3.53 μm component with size would imply that the emission from HD 97048 and Elias 1 originates from large neutral diamondoids. Interestingly, the work described here predicts that diamondoid cations have a band at 3.527 μm, suggesting that some of the emission from HD 97048 and Elias 1 could arise from diamondoid cations. The lack of characteristic diamondoid vibrational frequencies in the 5–16 μm region preclude these being used as interstellar diamondoid cation tracers.

We very gratefully acknowledge support from NASA's *Spitzer Space Telescope* Archival and Long Term Space Astrophysics Research Programs. A. R. thanks the NASA Exobiology program for its generous support. Y. L. acknowledges the REU 2006 program for support. We thank Anthony Jones, whose careful reading and detailed suggestions improved the manuscript.

REFERENCES

Adamson, A. J., Whittet, D. C. B., Chrysostomou, A., Hough, J. H., Kerr, T. H., Aiken, D.K, Wright, G., & Roche, P. F. 1999, ApJ, 512, 224
Allamandola, L. J., Sandford, S. A., Tielens, A. G. G. M., & Herbst, T. M. 1992, ApJ, 399, 134
———. 1993, Science, 260, 64
Allamandola, L. J., Tielens, A. G. G. M., & Barker, J. R. 1989, ApJS, 71, 733
Anders, E., & Zinner, E. 1993, Meteoritics, 28, 490
Basile, B. P., Middleditch, B. S., & Oro, J. 1984, Org. Geochem., 5, 211
Bauernschmitt, R., & Ahlrichs, R. 1996, Chem. Phys. Lett., 256, 454
Bauschlicher, C. W. 2002, ApJ, 564, 782
Bauschlicher, C. W., & Langhoff, S. R. 1997, Spectrochim. Acta, 53, 1225
Becke, A. D. 1993, J. Chem. Phys., 98, 5648
Braatz, A., Ott, U., Henning, Th., Jäger, C., & Jeschke, G. 2000, Meteoritics Planet. Sci., 35, 75
Bregman, J. D., & Temi, P. 2001, ApJ, 554, 126
Brooke, T. Y., Sellgren, K., & Geballe, T. R. 1999, ApJ, 517, 883
Brooke, T. Y., Sellgren, K., & Smith, R. G. 1996, ApJ, 459, 209
Chang, H.-C., Lin, J.-C., Wu, J.-Y., & Chen, K.-H. 1995, J. Phys. Chem., 99, 11081
Chen, G., Zhang, Y., He, D., & Zhang, F. 1990, Proc. SPIE, 1146, 229
Chiar, J. E., et al. 2006, ApJ, 651, 268
Chin, R. P., Huang, J. Y., Shen, Y. R., Chuang, T. J., Seki, H., & Buck, M. 1992, Phys. Rev. B., 45, 1522
Clemett, S. J., Maechling, C. R., Zare, R. N., Swan, P. D., & Walker, R. M. 1993, Science, 262, 721
Cox, P., & Kessler, M. F. 1999, The Universe as Seen by *ISO* (ESA SP-427; Noordwijk: ESA)
Cronin, J. R., & Chang, S. 1993, in The Chemistry of Life's Origins, ed. J. M. Greenberg, C. X. Mendoza-Gómez, & V. Pirronello (Dordrecht: Kluwer), 209
Dahl, J. E., Liu, S. G., & Carlson, R. M. K. 2003, Science, 299, 96
Dai, Z. R., Bradley, J. P., Joswiak, D. J., Brownlee, D. E., Hill, H. G. M., & Genge, M. J. 2002, Nature, 418, 157
Daulton, T. L., Eisenhour, D. D., Bernatowicz, T. J., Lewis, R. S., & Buseck, P. R. 1996, Geochim. Cosmochim. Acta, 60, 4853
Demyk, K., Dartois, E., d'Hendecourt, L., Jourdain de Muizon, M., Heras, A. M., & Breitfellner, M. 1998, A&A, 339, 553
Freund, M. M., & Freund, F. T. 2006, ApJ, 639, 210
Frisch, M. J., Pople, J. A., & Binkley, J. S. 1984, J. Chem. Phys., 80, 3265
Frisch, M. J., et al. 2003, Gaussian 03, Revision B.05 (Pittsburgh: Gaussian, Inc.)
Gudipati, M. S., & Allamandola, L. J. 2004, ApJ, 615, L177
Guillois, O., Ledoux, G., & Reynaud, C. 1999, ApJ, 521, L133
Habart, E., Natta, A., Testi, L., & Carbillet, M. 2006, A&A, 449, 1067
Halasinski, T. M., Weisman, J. L., Ruiterkamp, R., Lee, T. J., Salama, F., & Head-Gordon, M. 2003, J. Phys. Chem. A, 107, 3660
Hill, H. G. M., d'Hendecourt, L. B., Perron, C., & Jones, A. P. 1997, Meteoritics Planet. Sci., 32, 713
Hill, H. G. M., Jones, A. P., & d'Hendecourt, L. B. 1998, A&A, 336, L41
Hudgins, D. M., Bauschlicher, C. W., & Allamandola, L. J. 2005, ApJ, 632, 316
Jolibois, F., Klotz, A., Gadéa, F. X, & Joblin, C. 2005, A&A, 444, 629
Jones, A. P., & d'Hendecourt, L. B. 2000, A&A, 355, 1191
Jones, A. P., d'Hendecourt, L. B., Sheu, S. Y., Chang, H. C., Cheng, C. L., & Hill, H. G. M. 2004, A&A, 416, 235
Jørgenson, U. G. 1988, Nature, 332, 702
Jourdain de Muizon, M., D'Hendecourt, L. B., & Geballe, T. R. 1990, A&A, 235, 367
Kobashi, K., Nishimura, K., Miyata, K., Kawate, Y., Glass, J. T., & Williams, B. E. 1988, Proc. SPIE, 969, 159
Kouchi, A. Nakano, H. Y., Kimura, Y., & Kaito, C. 2005, ApJ, 626, L129
Lewis, R. S., Ming, T., Wacker, J. F., Anders, E., & Steel, E. 1987, Nature, 326, 160
Malloci, G., Joblin, C., & Mulas, G. 2007, Chem. Phys., 332, 353
Mattioda, A. L., Allamandola, L. J., & Hudgins, D. M. 2005, ApJ, 629, 1183
Mattioda, A. L., Hudgins, D. M., Bauschlicher, C. W., Rosi, M., & Allamandola, L. J. 2003, J. Phys. Chem. A, 107, 1486
Mutschke, H., Dorschner, J., Henning, Th., & Jager, C. 1995, ApJ, 454, L157
Nuth, J. A., & Allen, J. E. 1992, Ap&SS, 196, 117
Oomens, J., et al. 2006, J. Mol. Spectrosc., 238, 158
Peeters, E., Allamandola, L. J., Hudgins, D. M., Hony, S., & Tielens, A. G. G. M. 2004, in ASP Conf. Ser. 309, Astrophysics of Dust, ed. A. N. Witt, G. C. Clayton, & B. T. Draine (San Francisco: ASP), 141
Pirali, O., Vervloet, M., Dahl, J. E, Carlson, R. M. K., Tielens, A. G. G. M., & Oomens, J. 2007, ApJ, 661, 919

Roche, P. F., Allen, D. A, & Bailey, J. A. 1986, MNRAS, 220, 7P
Sandhu, G. S., Chu, W. K., Swanson, M. L., & Prins, J. F. 1988, Proc. SPIE, 969, 37
Saslaw, W. C., & Gaustad, J. E. 1969, Nature, 221, 160
Schutte, W. A., & Greenberg, J. M. 1997, A&A, 317, L43
Sellgren, K., Brooke, T. Y., Smith, R. G., & Geballe, T. R. 1995, ApJ, 449, L69
Stephens, P. J., Devlin, F. J., Chabalowski, C. F., & Frisch, M. J. 1994, J. Phys. Chem., 98, 11623
Stratmann, R. E., Scuseria, G. E., & Frisch, M. J. 1998, J. Chem. Phys., 109, 8218
Tielens, A. G. G. M., Seab, G. C., Hollenbach, D. J., & McKee, C. F. 1987, ApJ, 319, L109
Topalovic, R., Russell, J., McCombie, J., Kerr, T. H., & Sarre, P. J. 2006, MNRAS, 372, 1299
Van Kerckhoven, C. 2002, Ph.D. thesis, Katholieke Univ. Leuven, Belgium
Van Kerckhoven, C., Tielens, A. G. G. M., & Waelkens, C. 2002, A&A, 384, 568
Woon, D. E., & Park, J.-Y. 2004, ApJ, 607, 342